Rock Mech. Lett. **2025**, 2(2): 15

VANCE PRESS

Rock Mechanics Letters

www.journal-rml.com

Research Article

Analysis of Rock Friction Coefficient Characteristics Based on Friction Experimental Equipment

Zhipeng Hong[1*], Wei Hao[1], Liang He[1], Yinuo Zhang[1], Zhaoyu Wen[1]

[1] *State Key Laboratory of Eco-hydraulics in Northwest Arid Region, Xi'an University of Technology, 710048, China*
[*] Correspondence: 15171326135@163.com

Received: 20 May 2025
Revised: 6 June 2025
Accepted: 16 June 2025
Published date: 19 June 2025
Doi: 10.70425/rml.202502.15

Abstract: Friction coefficient, as a parameter of mechanical state, plays a crucial role in the shear failure of rocks in the field of Earth sciences. This paper investigates the frictional characteristics and anisotropy of rock by analyzing the coefficient of variation of the friction coefficient (f) and the anisotropy index of rock friction coefficients A_f. Rotational friction tests were conducted using cylindrical granite against square samples of granite, sandstone, and andesite in three directions to analyze the relationship between the friction coefficient and various drilling parameters. This study reveals the variations in the friction coefficient and notable changes in the friction coefficient's anisotropy. The results indicate a correlation between the alignment of turning points during the frictional stage and the rock strength. During the experiment, the friction coefficient undergoes cyclic variation before gradually stabilizing. The anisotropy of rotational friction follows the order: granite > andesite > sandstone, suggesting that the higher rock strength corresponds to greater frictional anisotropy. The rotational friction control coefficient C is derived and linked to the rotational friction stage. The duration of effective contact between rock surfaces and directional cutting efficiency are the primary factors contributing to anisotropy. The results offer practical implications for drilling design and seismic risk assessment in anisotropic rock formations.

Keywords: Rock; friction coefficient; anisotropy index; rock strength; drilling parameters

1. Introduction

Currently, research on rock sliding friction in petrology focuses on the micro medium and large based on the rock's physical characteristics [1]. At the micro scale, research focuses on the rock's internal cracks, including their formation, effects on friction, and underlying causes [2]. The medium scale is to study the rock as a macroscopic material, mainly to explore the friction mechanism of the rock and the size of the friction force, as well as the interaction mechanism between a single rock particle and the rock block [3]. When applied to actual production, its goal is to increase the favorable friction and eliminate the unfavorable friction. On a large scale, from a geographical perspective, the stability of geological structures is judged by analyzing the properties of rocks to explore the large-scale geographical faults, the movement and friction of continental plates, and the interaction forces between joints.

The traditional tectonic model of rock masses postulates a lithosphere comprised of a robust, brittle upper layer and a weaker, ductile lower layer, resulting in two forms of deformation: brittle fracture in the upper layer, leading to earthquakes, and ductile flow in the lower layer [4,5]. The coefficient of friction is a crucial mechanical parameter that plays a pivotal role in the shear failure of rocks within the field of earth science. This is especially significant as most earthquakes are triggered by the frictional sliding along faults. Hence, understanding the frictional properties of rocks is essential for gaining insights into seismic mechanics [6]. The friction coefficient is the most critical parameter affecting rock friction, and since rocks are heterogeneous materials, studying the anisotropy of the friction coefficient is of significant importance in understanding rock friction [7]. Rock anisotropy is the outcome of numerous geological processes, including sedimentary stress conditions, historical background, and fabricational processes [8–10]. Investigating the anisotropy of frictional coefficients holds significant importance in understanding rock friction [11]. Furthermore, the frictional behavior related to the shear rate and normal stress of rock discontinuities can significantly influence the dynamic response of rock masses [12]. Therefore, utilizing advanced digital drilling technology to collect detailed data allows for a more comprehensive investigation of their dynamic response.

However, no correlation model has yet been established linking this technology to rock friction. Given that friction plays a critical role in numerous rock engineering applications—such as fault slip, borehole stability, and excavation-induced deformation—this gap limits the broader applicability of digital drilling methods [13–15]. Rock friction is inherently complex, influenced by factors including lithology, mineral composition, surface roughness, and loading direction. Furthermore, the anisotropic nature of rock friction, which varies with drilling orientation, remains insufficiently explored through digital approaches [16]. To address this limitation, this study investigates the potential of digital drilling parameters to characterize frictional behavior and its anisotropy in different rock types. By integrating controlled friction experiments with real-time drilling data, we aim to establish a foundation for linking drilling parameters to rock friction coefficients [17–19]. This work provides a new perspective for extending digital drilling applications beyond strength assessment, enabling more comprehensive evaluations of rock mechanical behavior [1,16,20]. Yang et al. [21] developed a model for interparticle friction weakening during transport by conducting high-speed friction experiments simulating shear between adjacent particle surfaces. They found that the rapid increase in normal stress and shear velocity were the primary causes of the sharp decline in intergranular friction coefficients during the falling and collision stages [22]. In addition, they examined the frictional behavior of carbonate fracture surfaces and proposed two micromechanisms to explain the significant reduction in fault frictional resistance. These mechanisms account for the extremely low friction coefficients observed on carbonate fault surfaces. Qi et al. [23] estimated the impact of friction coefficient and crack density on the dynamic strength of specimens containing Mode I cracks by numerically solving dynamic equations for crack propagation, crack interaction, friction coefficient, and constitutive equations. Pirzada et al.[24] studied the relationship between rock joint friction behavior and contact surface area. They concluded that surface roughness (rock friction coefficient) cannot determine the shear behavior of rock joints when the actual contact area is not considered. Hellebrekers et al. [25] simulated the frictional characteristics of fault fissures to address the seismic behavior of long-English and mafic crystalline basement rocks from the Malawi Rift in the southern end of the East African Rift System (EARS). Ma et al. [26] established an analytical model for blocky rock systems, providing a profound analysis and study of their dynamic friction mechanisms. Chen et al. [27] analyzed the influence of roughness on the shear performance and acoustic emission characteristics of bonded rock-concrete interfaces. Guo et al. [28] conducted triaxial unloading tests on sandstone specimens using the RMT–150B rock mechanics testing system, analyzing the impact of end friction on rock mechanics parameters under different end friction factors and confining pressure unloading rates. Sun et al. [29] conducted experimental research on the shear mechanical characteristics of rock joints under different constant normal stiffness using the direct shear testing system RDS-200. Guo et al. [30] used FLAC3D to analyze the effects of lithological parameters, softening methods, mesh division, and loading rates on the stress-strain curve of cylindrical rock samples under uniaxial compression. They also analyzed the impact of rock sample scale, pore channels, and end friction effects based on optimized parameters. Wu et al. [31] studied the spatial variations of transverse anisotropy and evaluated them using the coefficient of variation (Cv) and anisotropy index (A_i) through digital borehole testing. He et al. [32] analyzed the correlation between rock burst tendency and friction characteristics. They established a relationship between residual elastic energy indicators and strength ratio and friction coefficient, determining the susceptibility of rock mass materials to rock bursts.

The main focus of this paper is to establish a correlation between rock friction characteristics and anisotropy. This paper investigates the frictional characteristics and anisotropy of rock by analyzing the coefficient of variation of the friction coefficient (f) and the anisotropy index of rock friction coefficients A_f. Rotational friction tests were conducted using cylindrical granite against square samples of granite, sandstone, and andesite in three directions to analyze the relationship between the friction coefficient and various drilling parameters. This study reveals the variations in the friction coefficient and notable changes in the friction coefficient's anisotropy.

2. Development of an analytical model

During the rotation-induced friction of the rock, it generates both horizontal and vertical forces, namely, the horizontal cutting force F_t and the horizontal centripetal force F_n, along with the vertical drilling pressure N. All these forces are interconnected with the rotational penetration. The rotational friction process can be divided into four distinct stages. The initial stage represents incomplete contact rotational friction, followed by the compacted rotational friction stage, the full contact rotational friction stage, and ultimately the static friction stage. During the incomplete contact stage of rotational friction testing, the uneven surface of natural rock leads to rock particles on the surfaces cutting against each other, with the dominant force being the cutting action. The compaction effect comes into play as a supplementary force. Initially, a rotary cutting instrument applies a vertical drilling force (N) and a fixed power rotation to the cylindrical rock, causing its lower surface to come into contact with the upper surface of the cubic rock and commence rotating. During this phase, side friction of the cylindrical rock can be disregarded, and therefore, the friction coefficient corresponds to the friction coefficient of its bottom surface.

With the ongoing increase in vertical drilling pressure, the surface particles on both rocks gradually become smoother. The cylindrical rock maintains its vertical rotation, and the test progresses into the compaction rotational friction stage. During this phase, compaction takes the lead, and the rocks break and experience rotating friction, allowing the cylindrical rock to continue moving forward. Simultaneously, the cut surface area of the square rock keeps expanding. The resulting friction, involving both the cylindrical rock's side and the square rock, cannot be overlooked. Thus, the friction coefficient becomes the sum of the friction coefficient f_1 on the bottom surface and the friction coefficient f_2 on the side wall.

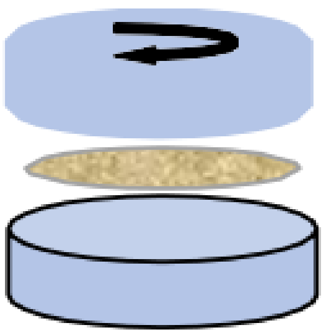

Figure 1. Rotational Friction Schematic

As the compacting rotational friction phase continues, the vertical and tangential rotational speeds of the cylindrical rock decrease progressively. When the vertical depth remains relatively constant, the test transitions into the full-contact rotational friction stage. Despite the ongoing increase in drilling pressure, the tangential speed keeps decreasing. Eventually, at a certain point, the speed abruptly drops to zero, marking the shift from full-contact rotational friction to the static friction stage. During this stage, as the drilling pressure continues to rise, the ultimate static friction force increases continuously. However, the cutting force is no longer capable of providing the power needed to keep the cylindrical rock rotating. Consequently, the friction force is no longer equal to the cutting force. A schematic diagram of the rock rotational friction process is shown in Fig.1.

Based on the drilling response model [14,33,34], the relationships between the following drilling parameters are introduced:the drilling pressure F (N), torque M (N·m),Speed of rotation ω (rpm), drilling speed v (mm/s) and depth s (mm) can be obtained, and ω can be converted to rad/s according to the test data.

$$F_t = \frac{M}{r} \tag{1}$$

$$f_1 = \frac{F_t}{N} \tag{2}$$

Bringing Equation (1) into Equation (2) yields:

$$f_1 = \frac{M}{rN} \tag{3}$$

In this test, the main vertical force is vertical drilling pressure, which is much greater than the gravity of cylindrical rock, so only vertical drilling pressure is considered when calculating the horizontal centripetal force, and according to the centripetal force formula, it can be obtained:

$$F_N = \frac{N\omega^2 r}{g} \tag{4}$$

In the above equation, g is the acceleration due to gravity, generally 9.8 (g/cm^2), and the sidewall friction coefficient is defined as f_2, which yields:

$$f_2 = \frac{F_t}{F_n} \tag{5}$$

Bringing equations (1) and (4) into equation (5) yields:

$$f_2 = \frac{Mg}{N\omega^2 r} \tag{6}$$

Defining the total coefficient of friction of the model as f, we get:

$$f = f_1 + f_2 \tag{7}$$

Bringing equations (3) and (6) into equation (7) yields:

$$f = \frac{M}{rN} + \frac{Mg}{N\omega^2 r} = \frac{M(\omega^2 + g)}{N\omega^2 r} \tag{8}$$

Due to the inconsistent elimination of anisotropy, the anisotropy of rocks manifests as directional responses in mechanical and physical behaviors [35–38]. The ratio of maximum to minimum strength, commonly used to represent strength anisotropy, fails to capture the influence of loading direction on rock strength [39]. Another method for calculating rock anisotropy is based on the variation in the longitudinal wave propagation velocity in rocks [40]. However, this method based on longitudinal wave velocity is only applicable to measuring the degree of anisotropy in dense rocks. In this study, the anisotropy of drilling characteristics is described as the directional deviation of friction coefficients between the X, Y, and Z directions, with the anisotropy index denoted as Af. The calculation formula is as follows:

$$A_f = \frac{f_x f_y + f_x f_z + f_y f_z}{f_x^2 + f_y^2 + f_z^2} \tag{9}$$

3. Experimental procedures

3.1 Specimen preparation

In a field exploration project near Shaanxi Province, China, rock samples were collected from different depths. Two rock samples were extracted from a borehole at a depth of approximately 700 meters (1st and 3rd samples in Fig. 2). These rocks are classified into two categories based on their formation conditions: ejective rocks (andesite) and intrusive rocks (granite) [41,42]. Another rock sample (2nd in Fig. 2) was obtained from a borehole at a depth of around 350 meters and is identified as a sedimentary rock [43]. This sedimentary rock is characterized as red sandstone, mainly based on the grain size. The granite primarily consists of minerals such as feldspar, quartz, and biotite, with quartz content ranging from 10% to 50%. Feldspar makes up about two-thirds of the total composition. Andesite has a composition similar to diorite and exhibits colors including dark gray, light pink, and dark brown, along with a speckled structure. Sandstone is predominantly formed by the cementation of sand grains, with the sand grain content exceeding 50%. Most of the sandstone is composed of quartz or feldspar. Conforming to the test procedures and precautions established by the International Society of Rock Mechanics (ISRM), cubic specimens of the three rock types were prepared, each measuring 50mm in length, width, and thickness.

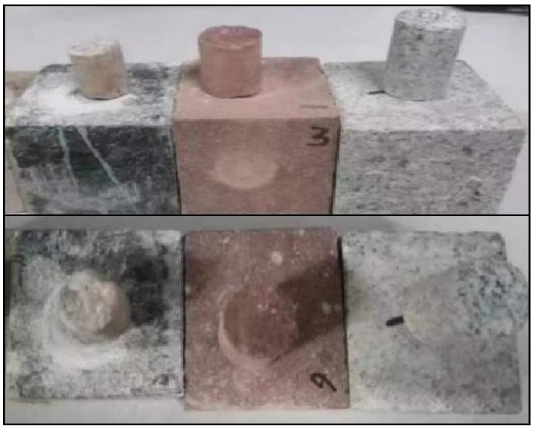

Figure 2. Specimens of three kinds of rocks

3.2 Testing system

In this testing process, an indoor friction experimental device was utilized, as illustrated in Fig. 3. This equipment is capable of precisely collecting key drilling parameters during the rock drilling process. These parameters include drilling pressure *F* in Newtons, torque *M* in Newton-meters, rotational speed w in revolutions per minute (rpm), drilling velocity (*v*) in millimeters per second (mm/s), and vertical displacement (*s*) in millimeters (mm). The frequency of data recording is set at 0.05 seconds. For the testing procedure, a diamond hollow drill bit with a 15mm inner diameter, 17mm outer diameter, and an effective drilling length of 50mm was employed. This drill bit is used to drill the cylindrical rock samples in contact with cubic rock specimens. The indoor digital drilling equipment is capable of swiftly and accurately measuring drilling parameters for small-scale rock samples, making it an efficient and time-saving tool. Furthermore, this system provides valuable reference data for obtaining rock sample parameters at construction sites. The collected drilling parameters are of sufficient accuracy to calculate friction parameters and study the friction characteristics and anisotropy of various rock types.

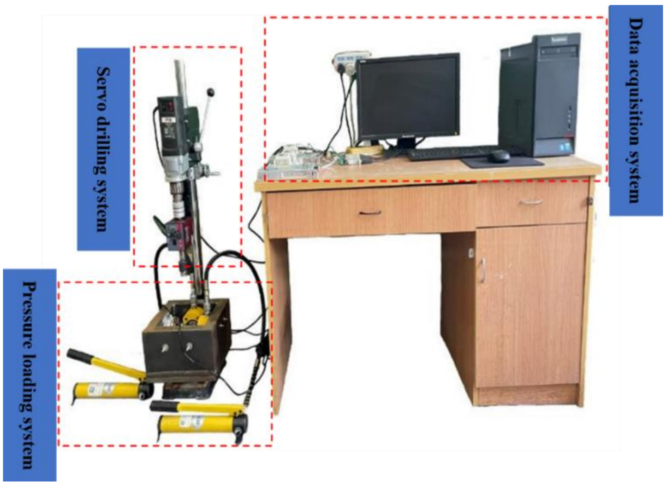

Figure 3. Schematic of Friction Experimental Equipment

3.3 Loading process

The frictional properties of rocks are influenced by numerous parameters. To simulate the rotational friction process between rocks, the following experimental steps are designed. Define three faces of the cube rock as 1, 2, and 3, as illustrated in Fig. 4. Perpendicular axes to these faces are designated as the X, Y, and Z axes, respectively. Conduct the experiment as follows:

(a) Secure the cylindrical rock onto the rotation apparatus of the digital drilling experimental equipment shown in Fig.3.

(b) Position the cube rock with the Z side facing upwards directly below the rotation apparatus. Adjust the position to ensure that the cylindrical rock is centered with respect to the cube rock.

(c) Initiate the digital drilling equipment while maintaining a constant instrument speed. Gradually increase the vertical drilling pressure and observe the rotational friction process of the rocks. Record the relevant data.

(d) When the rotation ceases, deactivate the rotation switch and remove the cube rock.

(e) Repeat steps (b), (c), and (d) for the X and Y surfaces of the rock to record the data.

(f) Replicate the above steps for cube rocks composed of other lithological materials.

These steps are designed to recreate and analyze the frictional behavior between different rock types during the rotational friction process.

The data processing of rock friction parameters is processed as follows:

Let h be the depth of each revolution, and we get:

$$h = \frac{2v}{60\omega} \tag{10}$$

Let ε be the vertical strain rate, and we can get:

$$\varepsilon = \frac{v}{s} \tag{11}$$

Let η be the tangential strain rate, yielding:

$$\eta = \frac{\omega}{n} \tag{12}$$

Where v is the drilling speed, s is the vertical displacement, ω is the rotation speed, and n (rad) is the total rotation volume. h (mm / rad) is each turn deep. ε is the vertical strain rate. η is the tangential strain rate.

$$s = \int_0^t v dt, n = \int_0^t \omega dt \tag{13}$$

The vertical displacement s is calculated by integrating the drilling speed v, and the total horizontal rotation n is calculated by integrating the speed ω. The rotational friction loading model is shown in Fig.4.

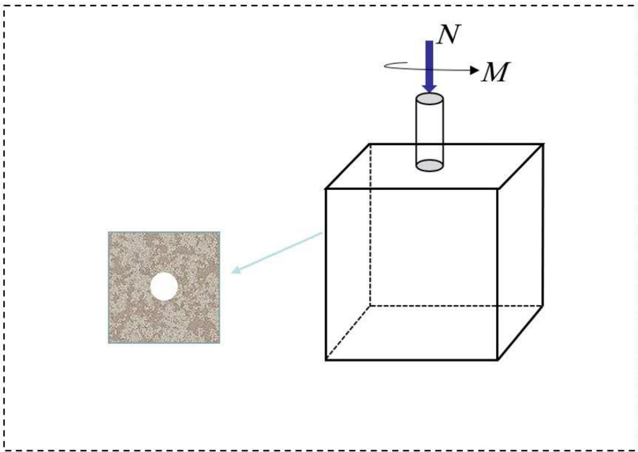

Figure 4. Schematic diagram of rockburst simulation test

4. Results

4.1 Rock Friction Coefficient

4.1.1 Three types of rock F_t-N curve analysis

Fig.5 illustrates the correlation between cutting force F_t and drilling pressure N for three different rock types in various directions. According to equation (8), we can derive the relationship between the rock's friction coefficient *f* and drilling pressure. As vertical drilling pressure intensifies, the rock undergoes continuous compression. It is evident from Fig. 5 that as vertical drilling pressure increases, horizontal cutting force F_t gradually rises. The friction coefficient *f* initially decreases and then begins to increase after reaching a critical point. The relationship curves between cutting force and drilling pressure show an upward trend for different rock types and directions throughout the entire rotary friction process. However, the rate of growth varies at different stages of rotary friction, as analyzed below: The drilling pressure loading ranges from 0 to 68 *N* in the Z-direction for sandstone spans. When the experiment reaches a completion rate of 80.9%, a sudden change in the curve indicates a transformation in the rotary friction stage. Within the drilling pressure range of 0 to 55 *N*, the F_t-*N* curve is convex, and the friction coefficient *f* continuously decreases with increasing drilling pressure. During this phase, the rotary friction of rock evolves from incomplete contact friction in the initial stages to compacted rotary friction until the drilling pressure reaches 55 *N*. Beyond this critical point, the compacted stage during rotary friction ends, and then the stage of full-contact rotary friction begins. When the drilling pressure ranges from 55 to 67 *N*, the F_t-*N* curve becomes concave, and the friction coefficient *f* continuously increases with increasing drilling pressure. During this phase, the rock undergoes full-contact rotary friction until *f* approaches +∞, marking the end of rock rotary friction and the onset of static friction. The variations in the X and Y directions of sandstone are similar to the Z-direction. In the X-direction, the experimental drilling pressure loading range for sandstone is 0 to 72 *N*, and it enters the full-contact rotary friction stage at 56 *N* of drilling pressure, with an experimental completion rate of 77.8%. In the Y-direction of sandstone, the experimental drilling pressure loading range is 0 to 59 *N*, and it enters the full-contact rotary friction stage at 52 *N* of drilling pressure, with an experimental completion rate of 88.1%.

Throughout the entire process of rotary friction drilling in sandstone, the magnitude of f is as follows: Y surface > Z surface > X surface. The phase transitions in granite and andesite are similar to those in sandstone, with slight variations. The experimental completions at the inflection points for granite in the Z, X, and Y directions are 90.2%, 73.7%, and 66.7%, respectively. During the rotary friction process in granite, the magnitude of the friction coefficient f is as follows: Y surface > Z surface > X surface.

For andesite, the inflection points in the Z, Y, and X directions have experimental completions of 46.2%, 53.6%, and 60.4%, respectively. During the rotary friction process in andesite, the magnitude of the friction coefficient f is as follows: Z surface > Y surface > X surface. The dashed line in the figure is defined as curve "*m*." In Fig. 5, curve "*m*" represents the collection of inflection points for the individual rocks in various directions within this experiment. The slope of the collection line for sandstone is negative, indicating that the inflection points of cutting force and friction coefficient for different surfaces of sandstone are negatively correlated with the drilling pressure at the inflection points. In contrast, for granite and andesite, the collection line has a positive slope, which is the opposite of sandstone. Therefore, the inflection points of cutting force and friction coefficient for different surfaces in granite and andesite are positively correlated with the drilling pressure at the inflection points.

From Fig. 5, it's also clear that during the rotary friction process, the friction coefficient *f* in andesite exhibits isotropy, meaning it shows similar behavior in all directions. This is because the slopes for X and Z directions in sandstone and granite are quite similar, resulting in *f* displaying transverse anisotropy. However, after the inflection points, the slopes of the three curves in all the graphs become quite similar, indicating that the friction *f* for all three types of rocks exhibits isotropy.

4.1.2 Analysis of *F*-*S* curves of three types of rocks

Fig. 6 illustrates the changing trends of the friction coefficient *f* in different directions for three types of rocks with respect to vertical displacements. In the rotary friction process in all three types of rocks and directions, when the two rocks initially come into contact, the friction coefficient *f* is initially high. As the vertical displacement *s* continues to increase, the friction coefficient *f* undergoes a sudden decrease, followed by a cyclical progression, and eventually stabilizes. Due to the fact that cubic rock formations result from the arrangement and combination of structural surfaces and bodies within the rock, expressing both the development and combination of structural surfaces within the rock and the size, geometric shape, and arrangement of structural bodies. During the process of rotary shearing, the uneven surfaces of the rock samples are continually smoothed by the shear action of the rock column, exposing new surfaces that continue to be smoothed by rotation. This process continues until the rock is compacted to a certain extent, at which point the internal arrangement and combination of the rock changes. The vertical drilling pressure remains relatively constant while the cutting force rapidly increases, gradually exceeding the realm of dynamic friction, causing the dynamic friction coefficient to begin to transition into the static friction coefficient.

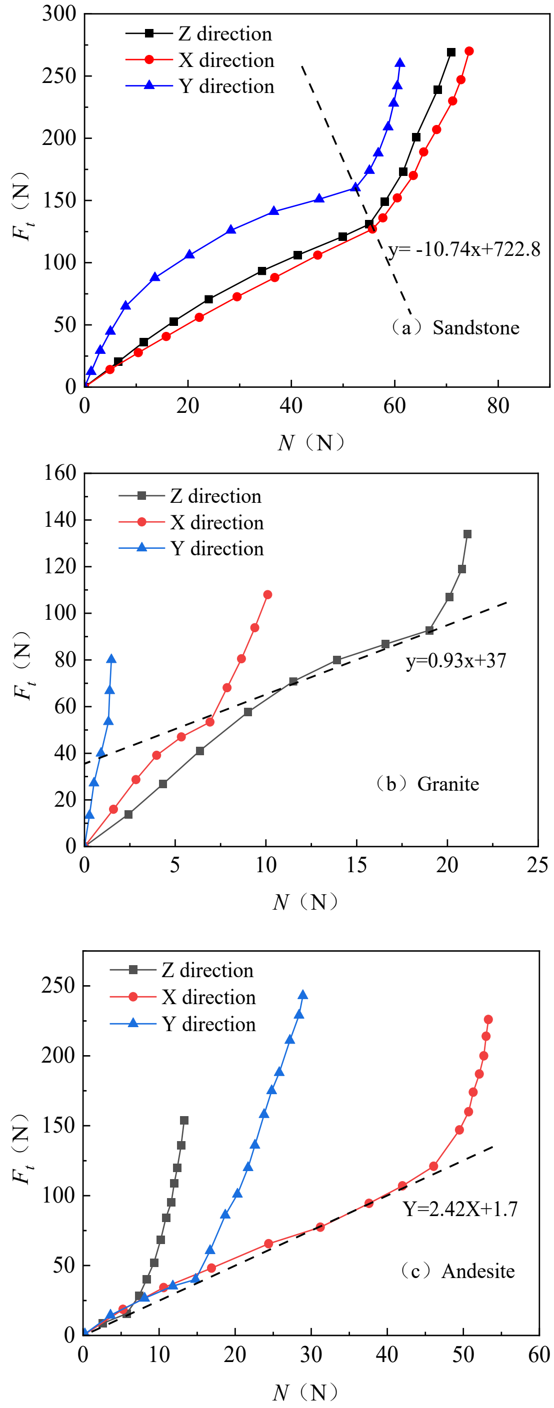

Figure 5. Curves of F_t - *N* for Three Types of Rocks. (a) Sandstone; (b) Granite; (c) Andesite.

In Fig. 6 (a), it shows the variation of the friction coefficient in three directions of sandstone with respect to vertical displacement. In the Z-direction, the friction coefficient decreases to a minimum at a vertical displacement of 0.6 mm, and it becomes stable at a vertical displacement of 1.7 mm. This indicates that the rotary friction phase transitions from incomplete contact friction to compacted friction when the rotation friction has progressed 35.3%. Between vertical displacements of 0.6 mm to 1.7 mm, the friction coefficient cyclically changes, and the rotary friction is in the compacted friction phase, with the experiment being 78.4% complete. When the vertical displacement exceeds 1.7 mm, the friction phase is in the full-contact friction stage, and the friction coefficient becomes stable and slowly increases. The changes in the X and Y directions of sandstone are similar to the Z-direction, and the trends in granite and andesite are mostly similar to those of sandstone.

Fig. 6 illustrates the relationship between the friction coefficient *f* and vertical displacement s in sandstone. This relationship is found to be entirely anisotropic during the incomplete contact and compacted friction phases. However, once it reaches the full-contact friction phase, it becomes isotropic, displaying similar behavior in all directions. In the case of granite, the *f-s* relationship exhibits transverse anisotropy throughout the entire rotary friction process. In contrast, for andesite, the *f-s* relationship demonstrates complete anisotropy throughout the entire rotary friction process, indicating distinct behavior in different directions, as opposed to uniform behavior in all directions.

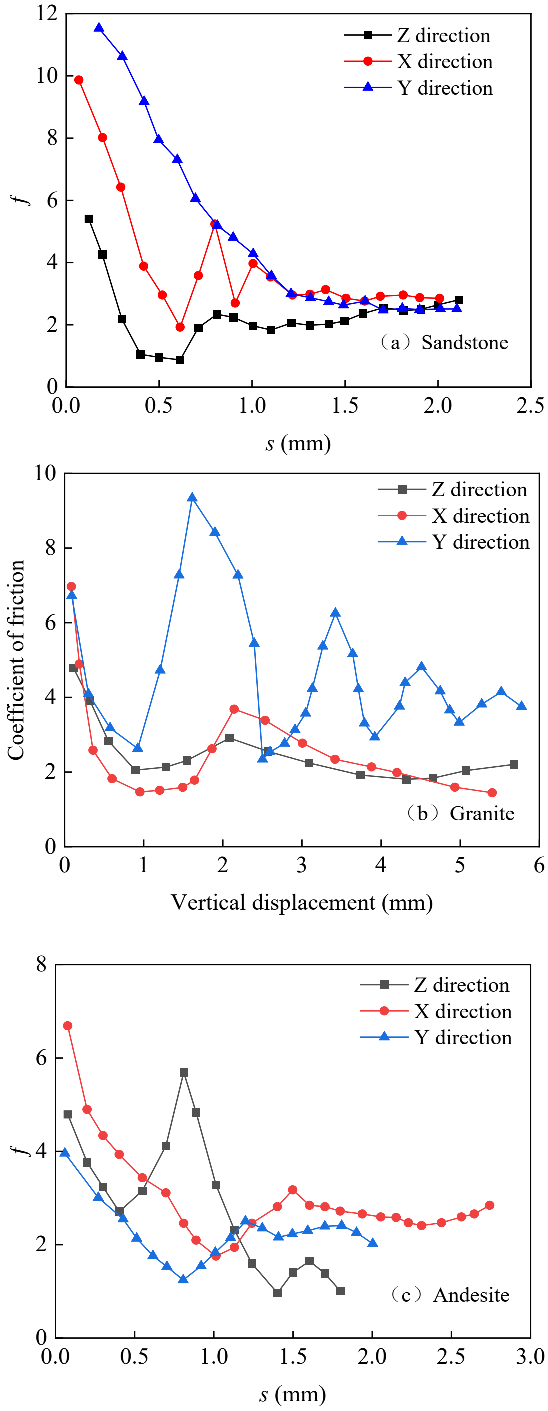

Figure 6. Curves of *f-s* for Three Types of Rocks. (a) Sandstone; (b) Granite; (c) Andesite.

4.1.3 The relationship between the friction coefficient in the Z-direction of sandstone and different parameters.

Fig. 7 depicts the relationship curves for the friction coefficient in the Z-direction of sandstone concerning each rotation depth, the correlation between the friction coefficient and the vertical strain rate, and the association between the friction coefficient and the tangential strain rate. These curves have been consolidated for clarity. Due to variations in the horizontal spans of these three curves, the horizontal axis of each curve has been adjusted, either enlarged or reduced, while maintaining a consistent vertical axis for a more intuitive representation.

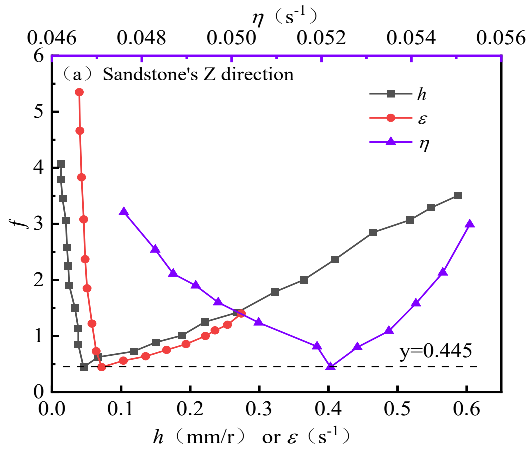

Figure 7. The relationship curve of the friction coefficient in the Z-direction of sandstone with three parameters

In the Z-direction of sandstone, the friction coefficient *f* initially exhibits a gradual decrease, starting from a relatively high value of 3.46 at a significant rotation depth (0.6mm). As the rotation depth (*h*) decreases, the friction coefficient f reaches its minimum point at *h*=0.045mm, where it plateaus at 0.445. Subsequently, as the rotation depth h further decreases, the friction coefficient experiences a rapid increase. The vertical strain rate in the Z-direction of sandstone also decreases from an initial value of 0.275 s^{-1}. The friction coefficient starts to gradually decrease from its initial value of 1.2 and reaches 0.445 at the inflection point, corresponding to a vertical strain rate of approximately 0.07 s^{-1}. As the vertical strain rate continues to decrease, the friction coefficient starts increasing at a higher rate. Similarly, the tangential strain rate in the Z-direction of sandstone decreases from its initial value of 0.595 s^{-1}. The friction coefficient gradually decreases from an initial value of 2.89 to 0.445 at the inflection point, coinciding with a tangential strain rate of approximately 0.405 s^{-1}. Subsequently, as the tangential strain rate continues to decrease, the friction coefficient begins to increase.

In Fig. 5, the dashed line represents the set of inflection points shared by the three curves, described by the equation y=0.445. This indicates that, on the same rock surface, as the experiment progresses and various parameters change, the corresponding minimum friction coefficient values remain constant. This observation validates that during the rotary friction process the initial phase involves incomplete contact and compacted friction. Over time, the friction coefficient steadily decreases until it reaches its minimum value. Subsequently, as the experiment progresses into the full-contact friction phase, the sliding friction transitions into static friction.

4.1.4 Analysis of *f-h* curves of three types of rocks

As the experiment advances, the rotation depth (*h*) steadily decreases, and the friction coefficient (*f*) initially follows a descending trend before subsequently rising. As discussed in previous sections, when the friction coefficient has not yet reached its minimum value, the experiment is in the phase of incomplete contact friction and compacted friction. However, when the friction coefficient reaches its nadir and initiates an upward trend, the experiment progresses into the full-contact friction phase and undergoes a transition to the static friction phase.

Fig. 8 (a) illustrates the behavior in the Z-direction of sandstone, where the friction coefficient f initiates a gradual decrease from a relatively high value of 0.63 at a significant rotation depth (0.0012 mm). As the rotation depth h decreases, at an experiment completion of 78.4%, the friction coefficient *f* reaches its nadir at *h*=0.00045mm (0.445). This signifies the conclusion of the incomplete contact friction and compacted contact friction phases. Subsequently, as the rotation depth h further decreases, the friction coefficient *f* experiences a rapid increase, continually deviating from the initial curve slope (tan135°). The experiment transitions into the full-contact friction phase and progresses to the static friction phase. The X and Y directions exhibit a similar trend. Fig. 8 (b) and 8 (c) reveal that the relationship between the friction coefficient and rotation depth in granite and andesite mirrors the behavior observed in sandstone.

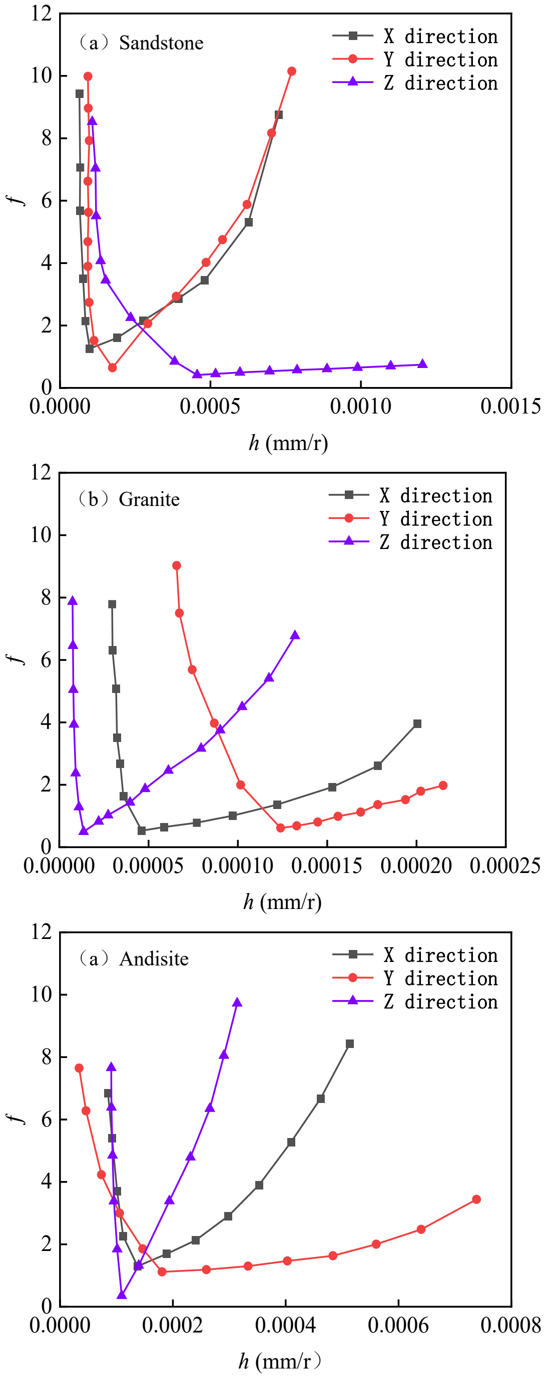

Figure 8. Curves of *f* -*h* for Three Types of Rock. (a) Sandstone; (b) Granite; (c) Andesite.

For sandstone, the friction coefficients in all three directions display transverse anisotropy in their variations with rotation depth. Whether it's during the stages of abrupt decrease or increase, the curves for the X and Y directions exhibit steeper slopes compared to the Z direction. Consequently, during the dynamic friction stage, the order of dynamic friction coefficients for andesite is X≈Y > Z. In the case of granite, the friction coefficients in all three directions demonstrate complete anisotropy in their variations with rotation depth. Both during the stages of abrupt decrease and increase, the curve for the Z direction is the steepest, followed by the X direction, with the Y direction having the slowest change. Therefore, during the dynamic friction stage in granite, the order of dynamic friction coefficients is Z > X > Y. Similarly, in andesite, the friction coefficients in all three directions also exhibit complete anisotropy in their variations with rotation depth. In both the stages of abrupt decrease and increase, the curve for the Z direction is the steepest, followed by the X direction, while the Y direction exhibits the slowest change. Consequently, during the dynamic friction stage in andesite, the order of dynamic friction coefficients is Z > X > Y.

4.1.5 Analysis of *f*-*ε* curves of three types of rocks

Fig.9 illustrates the relationship between the friction coefficient and vertical strain rate during the rotary friction process for three different types of rocks. Vertical strain rate represents the amount of vertical strain change within a unit of time. Vertical strain change is also correlated with drilling speed, meaning that drilling speed and vertical strain rate are positively related.

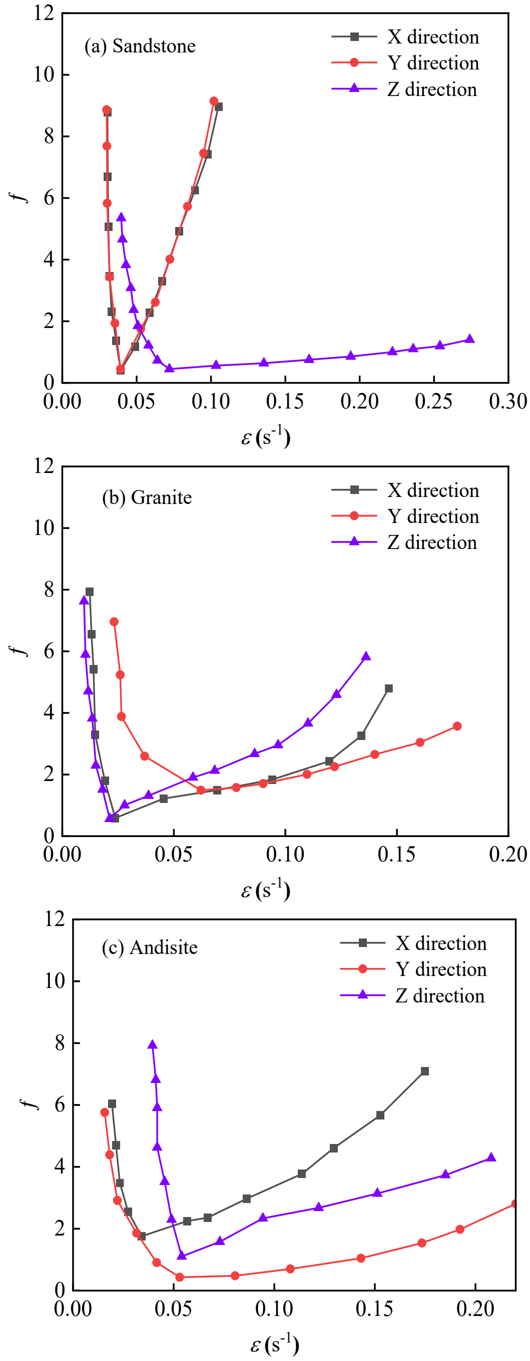

Figure 9. Curves of *f*-*ε* for Three Types of Rock. (a) Sandstone; (b) Granite; (c) Andesite.

As the experiment progresses, the drilling speed consistently decreases, resulting in a continuous decline in the vertical strain rate. As depicted in Figure 9 (a), when the vertical strain rate in the X-direction of sandstone decreases from its initial value of 0.095 s^{-1}, the friction coefficient experiences a sharp decrease from its initial value of 9 to 0.32, marking the inflection point. At this juncture, the vertical strain rate is approximately 0.04 s^{-1}, signifying the end of the incomplete contact and compacted friction phases. With further reduction in the vertical strain rate, the friction coefficient sharply increases with an almost vertical slope, indicating the onset of the full-contact friction phase. The patterns in the relationships for the Y and Z directions of sandstone resemble that of the X-direction. Fig. 9 (b) and 9 (c) reveal that the changes in the f-ε curves for granite and andesite also exhibit similarities to those of sandstone.

Sandstone is a sedimentary rock, whereas granite and andesite are both igneous rocks. Analyzing Fig. 9, it becomes evident that the friction coefficient vs. vertical strain rate relationship curves for the X and Y directions of sandstone remain quite similar across all stages of friction, but the curve for the Z direction significantly deviates from the other directions. Consequently, the curves for this rock exhibit transverse anisotropy throughout the entire experiment. In the cases of andesite and granite, the friction coefficient. vertical strain rate relationship curves for all three directions notably differ in the incomplete contact and compacted friction phases. However, during the transition from full-contact friction to static friction, the curves for two directions generally overlap. Consequently, the curves for these two types of rocks display complete anisotropy during the incomplete and compacted friction stages, but they demonstrate transverse anisotropy as they transition into static friction.

4.2 Analysis of f-η curves of three types of rocks

Fig. 10 illustrates the correlation between the friction coefficient and the tangential strain rate for the three rock types throughout the rotary shear process. The tangential strain rate signifies the amount of tangential strain occurring within a specific time interval. Furthermore, the tangential strain is associated with the rotation speed, as demonstrated by Eq. (13), which establishes a positive relationship between rotation speed and the tangential strain rate.

From Fig.10 (a), it can be observed that as the experiment progresses, the tangential strain rate in the X-direction of sandstone continuously decreases from an initial value of 0.054 s^{-1}. The friction coefficient starts decreasing from the initial value of 9.4 to 1.32, reaching the inflection point. This marks the end of incomplete contact friction and compacted friction. At this point, the tangential strain rate is approximately 0.0485 s^{-1}. As the tangential strain rate continues to decrease, the friction coefficient starts to increase, signifying the beginning of the full-contact friction phase.

The changes for the Y and Z directions of sandstone are similar to those of the X-direction. Fig.10 (b) and Fig.10 (c) demonstrate that the trends in the f-η curves for granite and andesite are also similar to those of sandstone.

Analysis of Fig. 10 reveals that the relationship between the friction coefficient and the tangential strain rate for the three directions of sandstone is consistently inconsistent throughout the entire experiment. Consequently, the curves for this type of rock exhibit complete anisotropy across the entire experimental duration.For granite, the f-η curves for all three directions maintain a striking similarity throughout the experiment, indicating that the tangential strain rate of granite displays complete isotropy in relation to the variation in the friction coefficient.In the case of andesite, notable discrepancies are observed in the f-η curves for all three directions during the dynamic friction phase. However, during the transition from full-contact friction to static friction, the curves for two directions tend to overlap. As a result, the curves for these two rock types exhibit complete anisotropy during the incomplete and compacted friction stages but display transverse anisotropy during the transition to static friction.

4.3 Anisotropy index of rock rotation friction

Prolonged contact time between the rock surface and the rotating cutter in a specific direction allows more extensive interaction between surface asperities. This extended interaction promotes increased micro-asperity deformation, grain interlocking, and localized compaction along that direction [44]. As a result, the frictional resistance becomes higher due to the accumulated microscopic damage and contact bonding, leading to directional dependency in the measured friction coefficient.

Fig.11 shows the anisotropy index of the friction coefficient for the three types of rocks as a function of drilling depth. In Fig.11 (a), for sandstone, the anisotropy index A_f of the friction coefficient is approximately 0.92 when the drill bit first contact with the rock sample. As the vertical drilling pressure advances, the anisotropy index A_f sharply decreases at a vertical displacement of 0.2 mm. At a vertical displacement of 0.5 mm, A_f reaches its minimum value (0.32). As the vertical displacement continues to increase, A_f starts to rise, reaching around 0.9 when the vertical displacement reaches 0.8 mm. Afterward, Af stabilizes at values between 0.95 and 1. The anisotropy is most significant for the sandstone used in this experiment at vertical displacements between 0.2 mm and 0.7 mm.

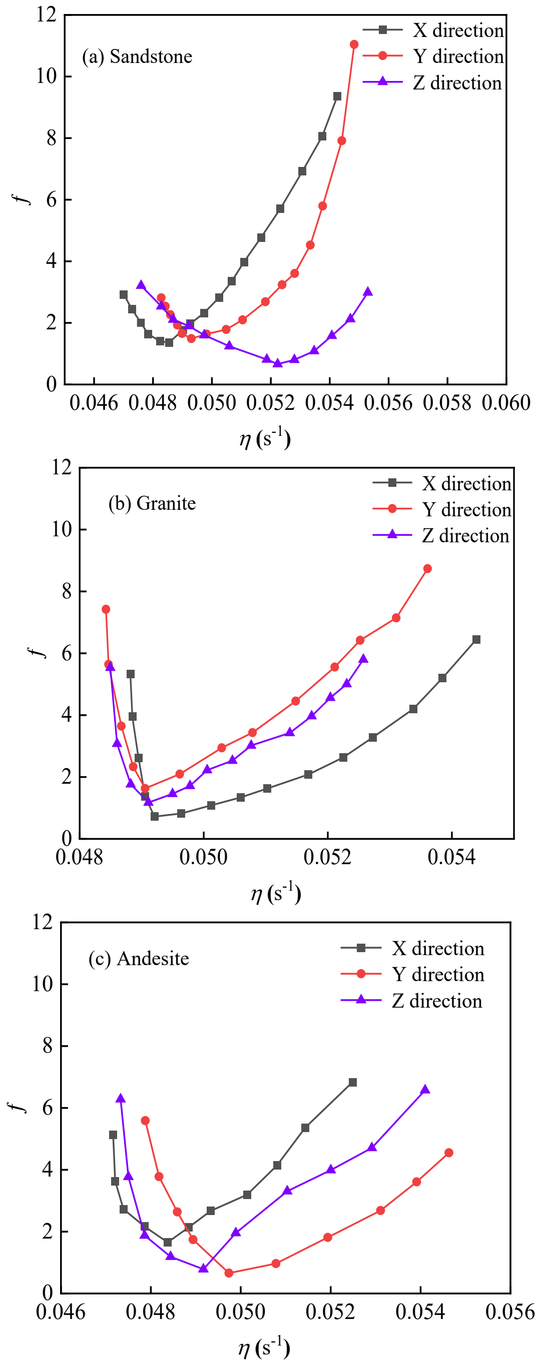

Figure 10. Curves of f-η for Three Types of Rock. (a) Sandstone; (b) Granite; (c) Andesite.

Fig.11 (b) reveals that the anisotropy index A_f of the friction coefficient for granite is approximately 0.92 when the drill bit initially engages with the rock sample during the rotational shear process. With increasing vertical drilling pressure and vertical displacement, A_f remains relatively stable at values between 0.8 and 0.9 for vertical displacements ranging from 0mm to 0.7 mm. However, once the vertical displacement surpasses 0.7 mm, the anisotropy index A_f begins to exhibit a cyclic decrease. This indicates that the anisotropy of the friction coefficient for the granite used in this experiment becomes more pronounced as the vertical displacement exceeds 0.7 mm.

Fig.11 (c) clearly shows that the anisotropy index A_f of the friction coefficient for andesite is approximately 0.98 when the drill bit first makes contact with the rock sample during the rotational shear process. As the vertical drilling pressure increases and vertical displacement grows, A_f begins to decrease around a vertical displacement of 0.25 mm. At a vertical displacement of 1.0 mm, the anisotropy index A_f reaches its minimum value (0.7). With further increases in vertical displacement, A_f starts to rise again, reaching approximately 0.98 at a vertical displacement of 1.2 mm, after which it stabilizes at values between 0.9 and 1. This illustrates that the anisotropy of the friction coefficient for the andesite used in this experiment is most prominent for vertical displacements between 0.2 mm and 1.2 mm. In summary, the anisotropy of rock rotational friction is observed as follows: granite > andesite > sandstone.

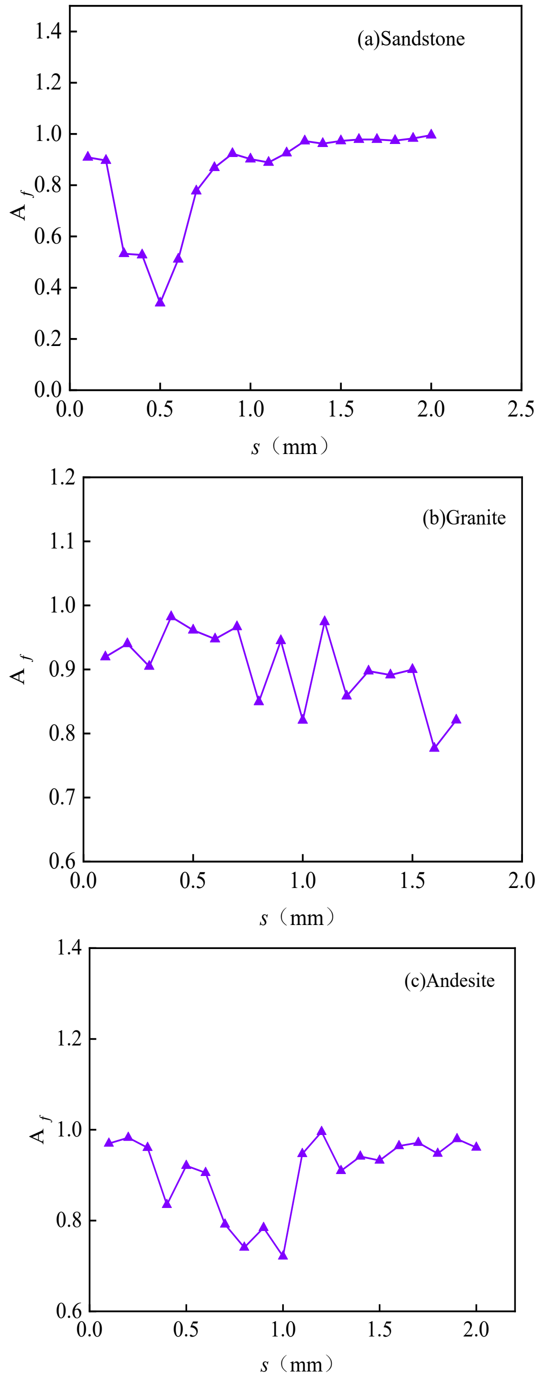

Figure 11. Curves of A_f -s for Three Types of Rock. (a) Sandstone; (b) Granite; (c) Andesite.

4.4 Curves m for three types of rocks.

The Fig. 12 illustrates the relationship between angle P and the rock's compressive strength Q.

Table 1. The values of k, P, Q of the three types of rocks

Rock types	Granite	Andisite	Sandstone
k	0.93	2.42	-10.74
P (°)	42.9	67.5	95.3
Q (MPa)	126	82	27

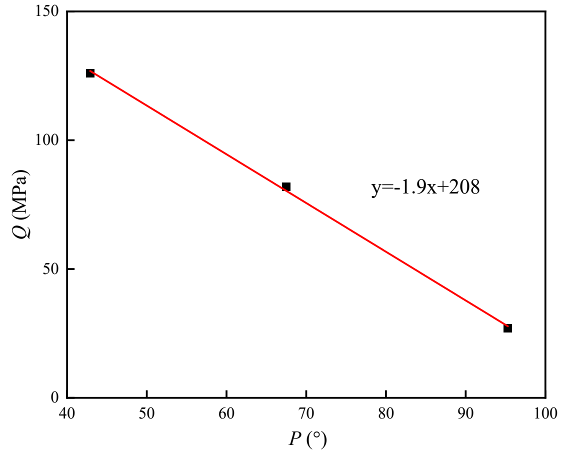

Figure 12. Graph depicting the relationship between P and Q

As shown in Fig. 12, angle P and compressive strength Q exhibit an inverse relationship. The fitted line has a slope of −1.9 and a y-intercept of 208. This indicates that as rock strength decreases, the slope of the frictional turning point trend line m becomes steeper.

4.5 The control parameters for the rock rotational friction process

Under a constant rotational speed setting, Eq. (8) implies that as drilling pressure increases, the rock continues to rotate and becomes increasingly compacted. This compaction increases the contact area along the borehole sidewalls, which in turn reduces the actual rotational speed. The rotational friction control coefficient C is defined as follows:

$$C = \frac{g}{\omega^2} \tag{14}$$

When $C < 1$,

$$\frac{Mg}{N\omega^2 r} < \frac{M\omega^2}{N\omega^2 r} \tag{15}$$

This is when the rock friction is primarily dominated by bottom friction.

When $C > 1$,

$$\frac{Mg}{N\omega^2 r} > \frac{M\omega^2}{N\omega^2 r} \tag{16}$$

and this is when the rock friction is primarily dominated by sidewall friction.

5. Discussion

This paper investigates the frictional characteristics and anisotropy of three types of rocks based on digital drilling technology. A rock rotational friction model is established according to the drilling response model. Mizoguchi et al. [40] conducted laboratory measurements of rock friction under seismic slip rates using a high-speed rotational shear friction device. Due to the variation of slip rates along the sample radius from zero at the center to a maximum at the circumference on the fault plane, they introduced the concept of "equivalent slip rate" (V) instead of slip rate. The relationship between the friction coefficient and equivalent slip rate under both wet and dry conditions was determined. The transitional phase plays a crucial role in promoting the instability of seismic or landslide fault slip. The experiment demonstrated an equivalent relationship between the friction coefficient during the rotational shear process and the slip friction coefficient. However, as rocks are heterogeneous materials, this experiment delves deeper into the rotational friction stage and the anisotropy of friction coefficients on this basis.

5.1 The stage of rock friction in the process of rotating friction

Xia et al., Baumberger and Ben-Davide [45–47] have demonstrated that the transition from static friction to sliding friction is mediated by rapid interface rupture. Building upon this, Passelègue et al. [48] established a connection between fracture mechanics and frictional motion. In this study, the frictional process of the model is subdivided into four distinct yet interrelated stages, based on principles of fracture mechanics [49]. These include: (1) the incomplete contact rotational friction stage, (2) the densification stage, (3) the full contact rotational friction stage, and (4) the static friction stage. These stages are identifiable through variations in the friction coefficient observed during the experiment.

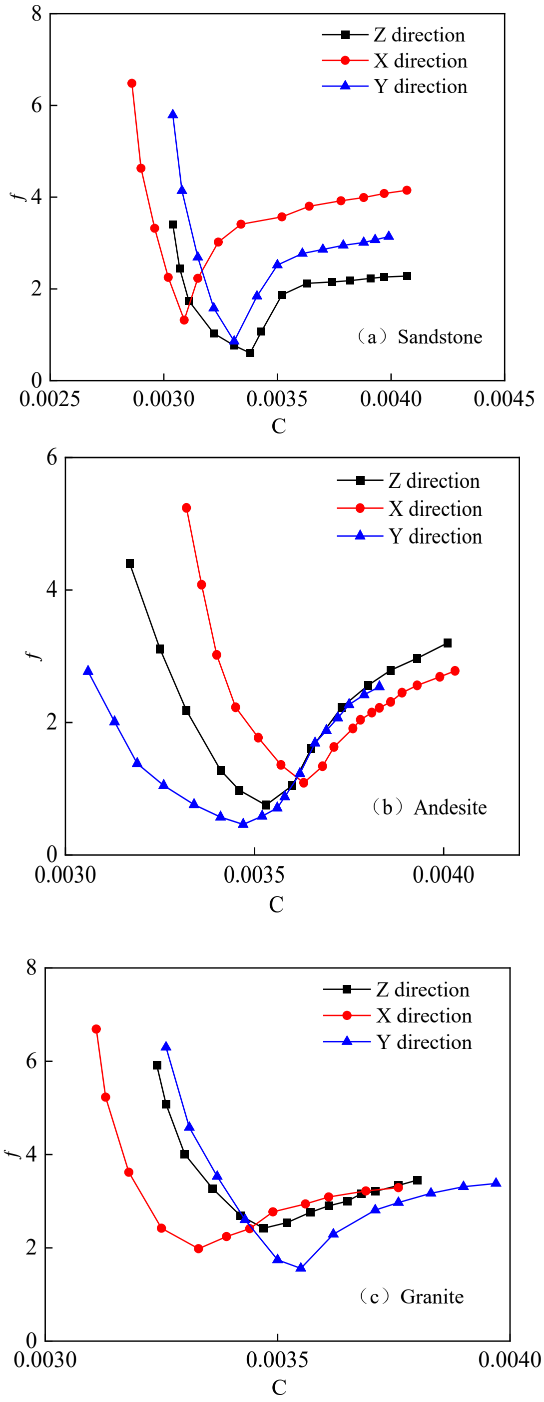

Figure 13. Curves of *f*-*C* for Three Types of Rock. (a) Sandstone; (b) Granite; (c) Andesite.

The friction coefficient of the rock in the experiment, denoted as $=[F_t(w^2+g)]/(Nw^2)$, undergoes continuous compaction throughout the entire experimental process. As the drilling pressure increases and the rotation speed w decreases, the friction coefficient f exhibits a trend of initially decreasing and then increasing with the progression of the rotational friction process. In other words, in the stages of incomplete contact and densification friction F_t, the growth rate is smaller than the growth rate of the vertical force N, while in the fully contact friction stage F_t, the growth rate is larger than the growth rate of N. This occurs because the transition from static to sliding friction requires an external force sufficient to alter the frictional state. When the rate of horizontal force increase gradually decreases while the frequency of vertical force increases rises, and the initial state is static friction, the static friction coefficient will gradually decline until it falls below the critical value, triggering a transition to sliding friction. Conversely, when the horizontal force increase rate accelerates and the vertical force frequency decreases, and the initial state is sliding friction, the sliding friction coefficient gradually increases until it exceeds the critical value, resulting in a transition back to static friction.

From the $f-h$ curves of the three types of rocks, it is evident that as the drilling depth h decreases, the friction coefficient f initially decreases until reaching a turning point, after which it increases. Analyzing the $f-\varepsilon$and $f-\eta$ curves for the three types of rocks reveals that as the vertical strain rate and tangential strain rate decrease, the friction coefficient initially decreases until a turning point and then increases.Through multiple verifications, it can be concluded that in the incomplete contact and densification friction stage, the initial dynamic friction, where the friction coefficient continuously decreases, transforms into dynamic friction where the coefficient starts to increase after reaching a minimum value at some point. This transition continues with the friction coefficient gradually increasing while the rate decreases, entering the fully contact friction stage. Ultimately, the rock specimen ceases rotation and enters the static friction stage. Analyzing the $f-s$ curves for the three types of rocks indicates that as the vertical displacement increases, the friction coefficient f exhibits a cyclic forward trend. The peak values of the cycles continuously decrease, ultimately stabilizing. This suggests that the transition between friction stages is most apparent when the two rocks first come into contact. As the compaction level of the rocks increases, the transformation of the friction coefficient becomes less pronounced, resulting in numerous friction cycles throughout the entire experimental process.The square rock specimen, characterized by the arrangement and combination of structural surfaces and bodies, represents the structural features of the rock mass, expressing both the development and combination of structural surfaces and the size, geometry, and arrangement of structural bodies. During the experiment, the uneven surface of the rock specimen is continuously sheared and ground by the rock column, exposing new surfaces. This process continues until the compaction reaches a certain level, causing a change in the arrangement and combination of the rock's interior. The growth of the vertical drilling pressure becomes significantly greater than the growth of cutting force, gradually exceeding the scope of dynamic friction. Internal features such as structural surfaces, fractures, and joints persist within the rock. However, as the number of friction cycles increases, the impact on the internal structure decreases, leading to smoother and more stable friction cycles.

5.2. Three kinds of rock friction coefficient anisotropy

Anisotropy refers to the directional variation of a material's chemical, physical, or other properties. It results in distinct material behaviors along different directions. It is a common characteristic in materials and media, exhibiting significant variations across multiple scales. Anisotropy is prevalent in systems ranging from crystalline structures and everyday materials to geological formations. This study focuses on the anisotropy of rock friction coefficients during rotational friction, investigating how it varies with changes in key parameters.

During the rotational friction process, prior to reaching the turning point, the friction coefficient of sandstone exhibits transverse isotropy with variations in drilling pressure. After the turning point, the friction coefficient demonstrates complete isotropy. The friction coefficient also displays transverse isotropy with changes in each drilling depth. Additionally, the relationship between the friction coefficient of sandstone and the vertical strain rate, as well as the tangential strain rate, exhibits transverse isotropy. As shown in Fig. 12, the anisotropy index of the sandstone friction coefficient varies with vertical displacement. Initially, the index changes sharply before stabilizing at approximately . The friction coefficient f, as a function of vertical displacement s, exhibits pronounced anisotropy during the initial cycling stage and transitions to isotropy during the stable stage.

Throughout the entire rotational shear process of granite, the friction coefficient consistently exhibits complete anisotropy with variations in drilling pressure. The friction coefficient also displays complete anisotropy with each drilling depth. During the dynamic friction stage, it shows complete anisotropy, transitioning to transverse isotropy during the transformation from dynamic to static friction. From Fig. 12, it can be observed that the anisotropy index of the friction coefficient for granite undergoes significant variations with vertical displacement, ultimately stabilizing at around 0.85. Considering the comprehensive curves, the friction coefficient f in relation to vertical displacement s demonstrates transverse isotropy in all cycling stages. The drastic fluctuations in the friction coefficient anisotropy index throughout the entire process can be attributed to the significant variations in the friction coefficient on the Y surface.

Andesite and granite both belong to igneous rocks and share many similarities. The friction coefficient, with variations in drilling pressure, initially exhibits transverse isotropy in the initial stage, transitioning to complete isotropy after the turning point. The friction coefficient also demonstrates complete anisotropy with each drilling depth. During the dynamic friction stage, it shows complete anisotropy, transitioning to transverse isotropy during the transformation from dynamic to static friction. For andesite, the anisotropy index of the friction coefficient changes significantly during the initial stage of vertical displacement. It first decreases to a minimum, then increases and stabilizes at approximately 0.95. Based on the overall trend, the friction coefficient f as a function of vertical displacement s, exhibits pronounced anisotropy throughout all cycling stages, ultimately stabilizing with transverse isotropy.

In a comprehensive analysis, during the incomplete contact and densification friction stage, the friction coefficients of the three types of rocks in this experiment exhibit pronounced anisotropy with variations in various parameters. In the fully contact friction stage, the three types of rocks used in this experiment demonstrate stable anisotropy. Moreover, as the compressive strength of the rocks increases, the anisotropy of the friction coefficients becomes more pronounced.

5.3. Discussion on the turning point of friction coefficient

In Section 4.1, the collective lines of turning points for each direction of an individual rock are summarized, with x representing drilling pressure *N* and y representing horizontal cutting force F_t. This indicates that the turning points of the friction coefficients in each direction of the rock are inversely proportional to the drilling pressure. As drilling pressure increases, the friction coefficients of the turning points in each direction of the rock show a trend of inversely proportional decrease.

From Section 4.3, it can be concluded that there is a correlation between the collective lines of turning points for the friction stages in the three directions of the square rock and the compressive strength of the rock.

In this study, square rock samples were used, and the friction locations were all at the centers of the rock faces. From Fig. 5, there is a correlation between the turning points of friction coefficients in the three perpendicular directions. Considering that the friction coefficient is primarily related to the roughness of the rock surface, and surface roughness is mainly influenced by the rock's cementation degree, jointing, and fissures, which are in turn influenced by structural surfaces, it is hypothesized that the turning points of friction coefficients in each direction of the rock have a geometric relationship with the angle between that direction and the structural surface.

6. Conclusions

This study, based on digital drilling technology, conducted rotational friction tests on square rock samples in various directions, established a theoretical model, and analyzed the experimental data. The conclusions drawn from the analysis are summarized as follows:

Rotational friction in rocks progresses through distinct stages—from incomplete contact to static friction—and exhibits cyclic behavior with peak friction occurring in the early stages. A theoretical model was established to describe these stages and their transitions.

Significant anisotropy in friction coefficients was observed, correlating with rock type and compressive strength (Granite > Andesite > Sandstone). An anisotropy index was introduced to quantify this behavior and its implications for geological processes.

The rotational friction control coefficient was proposed to characterize the transition of dominant friction from bottom to sidewall. This coefficient, along with observed turning points, provides insight into how rock properties affect frictional behavior under drilling conditions.

Author contributions

Conceptualization, Z.H.; methodology, W.H.; validation, L.H., formal analysis, Z.W.; investigation, Z.H; data curation, Z.H; writing — original draft preparation, Z.H; writing — review and editing, W.H; visualization, Y.Z.; supervision, W.H and Y.Z.; project administration, Y.Z. and L.H. All authors have read and agreed to the published version of the manuscript.

Acknowledgments

No funding was received to assist with the preparation of this manuscript.

Conflicts of Interest

All the authors claim that the manuscript is completely original. The authors also declare no conflict of interest.

Data availability

All relevant data related to this manuscript are available and can be provided upon reasonable request.

References

1. Roxborough FF, Phillips HR. Rock excavation by disc cutter. International Journal of Rock Mechanics and Mining Sciences & Geomechanics Abstracts. 1975; 12(12): 361–6. Doi:10.1016/0148-9062(75)90547-1
2. Wang Q, Liu B, Jiang B, Gao H, Li S, Xu S, et al. Application of slip line theory and core drilling in the prediction of rock *c-φ* parameters. European Journal of Environmental and Civil Engineering. 2022; 26(6): 2204–17. Doi:10.1080/19648189.2020.1755369
3. Wang Q, Gao S, Jiang B, Li S, He M, Gao H, et al. Rock-Cutting Mechanics Model and Its Application Based on Slip-Line Theory. Int J Geomech. 2018; 18(5): 04018025. Doi:10.1061/(ASCE)GM.1943-5622.0001136
4. Cowie PA, Scholz CH. Growth of faults by accumulation of seismic slip. Journal of Geophysical Research: Solid Earth. 1992; 97(B7): 11085–95. Doi:10.1029/92JB00586
5. Scholz CH. Wear and gouge formation in brittle faulting. Geology. 1987; 15(6):493–5. Doi:10.1130/0091-7613(1987)15<493:WAGFIB>2.0.CO;2
6. Han R, Hirose T, Shimamoto T, Lee Y, Ando J. Granular nanoparticles lubricate faults during seismic slip. Geology. 2011; 39(6): 599–602. Doi:10.1130/G31842.1
7. Ramamurthy T, Rao GV, Singh J. Engineering behaviour of phyllites. Engineering Geology. 1993; 33(3):209–25. Doi:10.1016/0013-7952(93)90059-L
8. Amadei B. Importance of anisotropy when estimating and measuring in situ stresses in rock. International Journal of Rock Mechanics and Mining Sciences & Geomechanics Abstracts. 1996; 33(3): 293–325. Doi:10.1016/0148-9062(95)00062-3
9. Hoek E, Marinos PG, Marinos VP. Characterisation and engineering properties of tectonically undisturbed but lithologically varied sedimentary rock masses. International Journal of Rock Mechanics and Mining Sciences. 2005; 42(2): 277–85. Doi:10.1016/j.ijrmms.2004.09.015
10. Oda M, Nakayama H. Yield Function for Soil with Anisotropic Fabric. Journal of Engineering Mechanics. American Society of Civil Engineers; 1989; 115(1): 89–104. Doi:10.1061/(ASCE)0733-9399(1989)115:1(89)
11. Sayers CM. Stress-dependent seismic anisotropy of shales. GEOPHYSICS. Society of Exploration Geophysicists; 1999; 64(1):93–8. Doi:10.1190/1.1444535
12. Kuganenthira N, Zhao D, Anandarajah A. Measurement of fabric anisotropy in triaxial shearing. Géotechnique. ICE Publishing; 1996; 46(4): 657–70. Doi:10.1680/geot.1996.46.4.657
13. Munoz H, Taheri A, Chanda E. Rock cutting characteristics on soft-to-hard rocks under different cutter inclinations. International Journal of Rock Mechanics and Mining Sciences. 2016; 87: 85–9. Doi:10.1016/j.ijrmms.2016.05.014
14. Munoz H, Taheri A, Chanda EK. Rock Drilling Performance Evaluation by an Energy Dissipation Based Rock Brittleness Index. Rock Mech Rock Eng. 2016; 49(8): 3343–55. Doi:10.1007/s00603-016-0986-0
15. Richard T, Dagrain F, Poyol E, Detournay E. Rock strength determination from scratch tests. Engineering Geology. 2012; 147–148: 91–100. Doi:10.1016/j.enggeo.2012.07.011
16. Kalantari S, Hashemolhosseini H, Baghbanan A. Estimating rock strength parameters using drilling data. International Journal of Rock Mechanics and Mining Sciences. 2018; 104: 45–52. Doi:10.1016/j.ijrmms.2018.02.013
17. Liu Y, Ma T, Chen P, Yang C. Method and apparatus for monitoring of downhole dynamic drag and torque of drill-string in horizontal wells. Journal of Petroleum Science and Engineering. 2018; 164: 320–32. Doi:10.1016/j.petrol.2018.01.077
18. Ma T, Chen P, Han X. Simulation and interpretation of the pressure response for formation testing while drilling. Journal of Natural Gas Science and Engineering. 2015; 23: 259–71. Doi:10.1016/j.jngse.2015.01.044
19. Schunnesson H. RQD predictions based on drill performance parameters. Tunnelling and Underground Space Technology. 1996; 11(3): 345–51. Doi:10.1016/0886-7798(96)00024-7
20. Hareland G, Wu A, Rashidi B. A Drilling Rate Model for Roller Cone Bits and Its Application. OnePetro; 2010. Doi:10.2118/129592-MS
21. Yang L, Zhang M, Jiao W, Wu Y, Zhang C, Wang Z. Influence of intergranular friction weakening on rock avalanche dynamics. Computers and Geotechnics. 2023; 159: 105440.
22. Zhang M, Yang L, Li W, Wang Z, Zhang C, Chen Q, et al. Frictional properties of the rupture surface of a carbonate rock avalanche. International Journal of Rock Mechanics and Mining Sciences. 2022; 153:105088.
23. Qi C, Xia C, Dyskin A, Zhao F. Effect of crack interaction and friction on the dynamic strength of rock-like materials with many cracks. Engineering Fracture Mechanics. 2021; 257: 108006. Doi:10.1016/j.engfracmech.2021.108006
24. Pirzada MA, Roshan H, Sun H, Oh J, Andersen MS, Hedayat A, et al. Effect of contact surface area on frictional behaviour of dry and saturated rock joints. Journal of Structural Geology. 2020; 135: 104044.
25. Hellebrekers N, Niemeijer AR, Fagereng Å, Manda B, Mvula RL. Lower crustal earthquakes in the East African Rift System. Tectonophysics. 2019; 767: 228167.

26. Ma GW, An XM, Wang MY. Analytical study of dynamic friction mechanism in blocky rock systems. International Journal of Rock Mechanics and Mining Sciences. 2009; 46(5): 946–51. Doi:10.1016/j.ijrmms.2009.04.001
27. Chen Y, Yang J, Li M, Zhou L, Guo B, Zuo J. Effects of roughness on shear properties and acoustic emission characteristics of bonded Rock-Concrete interfaces. Construction and Building Materials. 2023; 398:132405.
28. Guo JB, Guo BH, Chen Y, Luo T. Strength criterion for rock unloading considering end friction effect. Chinese Journal of Rock Mechanics and Engineering. 2019; 38(7): 1307–18. Doi:10.13722/j.cnki.jrme.2018.1433
29. Sun CX, Guo BH, Cheng T, Tian SX, Sun JH. Experimental study on shear mechanical behavior of rock joints under constant normal stiffness. China Sciencepaper Online. 2021; 14(1): 114–23
30. Guo BH. Numerical analysis of sample size, borehole, and end friction effects in rock specimens. Chinese Journal of Rock Mechanics and Engineering. 2009; 28(S2): 3391–401.
31. Wu K, He M, Yuan Z, Liu X, Luo B, Ma X, et al. Characterizing rock transverse anisotropic spatial variations using digital drilling. Geoenergy Science and Engineering. 2024; 232: 212451. Doi:10.1016/j.geoen.2023.212451
32. He M, Zhang Z, Zhu J, Li N, Li G, Chen Y. Correlation between the rockburst proneness and friction characteristics of rock materials and a new method for rockburst proneness prediction. Journal of Petroleum Science and Engineering. 2021; 205:108997.
33. He M, Wang H, Ma C, Zhang Z, Li N. Evaluating the Anisotropy of Drilling Mechanical Characteristics of Rock in the Process of Digital Drilling. Rock Mech Rock Eng. 2023; 56(5): 3659–77. Doi:10.1007/s00603-023-03242-1
34. Lhomme T. Frictional contact at a rock-tool interface [PhD Thesis]. University of Minnesota; 1999.
35. Thomsen L. Weak elastic anisotropy. Geophysics. 1986; 51(10): 1954–66. Doi:10.1190/1.1442051
36. Ramamurthy T. Strength and modulus responses of anisotropic rocks. Comprehensive Rock Engineering. Pergamon Press Oxford, UK; 1993; 1(13): 313–29.
37. Gurevich B, Pervukhina M, Makarynska D. An analytic model for the stress-induced anisotropy of dry rocks. Geophysics. 2011; 76(3): WA125–33. Doi:10.1190/1.3567950
38. Shen B, Siren T, Rinne M. Modelling Fracture Propagation in Anisotropic Rock Mass. Rock Mech Rock Eng. 2015; 48(3): 1067–81. Doi:10.1007/s00603-014-0621-x
39. Rubinstein SM, Cohen G, Fineberg J. Detachment fronts and the onset of dynamic friction. Nature. Nature Publishing Group UK London; 2004; 430(7003): 1005–9.
40. Mizoguchi K, Fukuyama E. Laboratory measurements of rock friction at subseismic slip velocities. International Journal of Rock Mechanics and Mining Sciences. 2010; 47(8):1363–71.
41. Li Z, Fortin J, Nicolas A, Deldicque D, Guéguen Y. Physical and Mechanical Properties of Thermally Cracked Andesite Under Pressure. Rock Mech Rock Eng. 2019; 52(10): 3509–29. Doi:10.1007/s00603-019-01785-w
42. Chen Y-L, Ni J, Shao W, Azzam R. Experimental study on the influence of temperature on the mechanical properties of granite under uni-axial compression and fatigue loading. International Journal of Rock Mechanics and Mining Sciences. 2012; 56: 62–6. Doi:10.1016/j.ijrmms.2012.07.026
43. Xia B, Li Y, Hu H, Luo Y, Peng J. Effect of Crack Angle on Mechanical Behaviors and Damage Evolution Characteristics of Sandstone Under Uniaxial Compression. Rock Mech Rock Eng. 2022; 55(11): 6567–82. Doi:10.1007/s00603-022-03016-1
44. Lu P, Wood RJK, Gee MG, Wang L, Pfleging W. The use of anisotropic texturing for control of directional friction. Tribology International. 2017; 113: 169–81. Doi:10.1016/j.triboint.2017.02.005
45. Xia K, Rosakis AJ, Kanamori H, Rice JR. Laboratory Earthquakes Along Inhomogeneous Faults. Science. American Association for the Advancement of Science; 2005; 308(5722): 681–4. Doi:10.1126/science.1108193
46. Baumberger T, Caroli C, Ronsin O. Self-healing slip pulses and the friction of gelatin gels. Eur Phys J E. 2003; 11(1): 85–93. Doi:10.1140/epje/i2003-10009-7
47. Ben-David O, Cohen G, Fineberg J. The Dynamics of the Onset of Frictional Slip. Science. 2010; 330(6001): 211–4. Doi:10.1126/science.1194777
48. Passelègue FX, Schubnel A, Nielsen S, Bhat HS, Madariaga R. From Sub-Rayleigh to Supershear Ruptures During Stick-Slip Experiments on Crustal Rocks. Science. 2013; 340(6137): 1208–11. Doi:10.1126/science.1235637
49. Bayart E, Svetlizky I, Fineberg J. Fracture mechanics determine the lengths of interface ruptures that mediate frictional motion. Nature Physics. Nature Publishing Group UK London; 2016; 12(2):166–70.